Tikrit Journal of Engineering Sciences (2025); 32(4): 2259
DOI: http://doi.org/10.25130/tjes.32.4.7

IRAQI Academic Scientific Journals

ISSN: 1813-162X (Print); 2312-7589 (Online)

Tikrit Journal of Engineering Sciences

available online at: http://www.tj-es.com

TJES Tikrit Journal of Engineering Sciences

Shear Capacity-Curvature Ductility Relationship of High-Strength Concrete Cantilever Beam of Different Failure Modes

Hussein A. Merie *, Mazin B. Abdul-Rahman, Wisam A. Aules

Civil Department, Engineering College, Tikrit University, Tikrit, Iraq.

Keywords:
Cantilever beam; Curvature ductility; High-strength concrete; Shear capacity; Mode of failure.

Highlights:

- *Shear capacity of the high-strength concrete cantilever beam.*
- *General behavior of the plastic hinge region with different failure modes.*
- *Shear capacity-curvature ductility relationship.*

ARTICLE INFO

Article history:

Received	11 July 2024
Received in revised form	15 Aug. 2024
Accepted	19 Sep. 2024
Final Proofreading	25 Aug. 2025
Available online	29 Aug. 2025

Citation: Merie HA, Abdulrahman MB, Aules WA. **Shear Capacity-Curvature Ductility Relationship of High-Strength Concrete Cantilever Beam of Different Failure Modes**. *Tikrit Journal of Engineering Sciences* 2025; **32**(4): 2259.
http://doi.org/10.25130/tjes.32.4.7

**Corresponding author:*

Hussein A. Merie

Civil Department, Engineering College, Tikrit University, Tikrit, Iraq.

Abstract: This research investigated the shear capacity and curvature ductility relation of high-strength reinforced concrete cantilever beams subjected to monotonic loading. Twelve cantilever beams with section dimensions of 200×300 mm were tested. The study determined the impact of factors, such as span-to-effective depth ratios "a/d", stirrup spacing, compressive strength, and longitudinal reinforcement, on the behavior of the beam at the plastic hinge with various failure modes, i.e., flexural, shear, and combined. The specimens were divided into 4 groups, each containing 3 beams and 3 values for each variable. Strain gauges (SG) and Linear Variable Differential transformers (LVDTs) were used to measure the strains and deflections. In the first test group, as the a/d ratio increased from 750 to 850 and then to 1150 mm, shear capacity rose by 23% and 28%, while curvature ductility improved by 88% and 112%, with failure modes including shear, combined, and flexural, showing a direct and semi-linear relationship between curvature ductility and shear capacity. Increasing stirrup spacing from 100 to 150 and then to 300 led to a 59.7% and 73.5% drop in shear capacity, respectively, and a 15.3% and 62.5% reduction in curvature ductility, respectively, indicating a direct nonlinear relationship, with a change in failure mode from flexural, combined, and shear. The third group, with compressive strength values of 50.3, 55, and 65 MPa, exhibited a decrease in shear capacity of 8.17% and 9.13%, accompanied by an increase in curvature ductility of 20.17% and 153%. However, the relationship between these parameters was unclear. Moreover, the specimens showed different failure modes. The fourth group investigated longitudinal steel with ratios of 0.234, 0.6578, and 0.5555. As the ratios increased, shear capacity decreased from 34.8% to 53.2%, and the curvature ductility declined from 55.5% to 82.13%. The results revealed a direct linear relationship as the failure modes transitioned among flexural, combined, and shear.

العلاقة بين سعة القص ومطيلية التقوس للعتبات الكابولية الخرسانية المسلحة عالية المقاومة مع انماط فشل مختلفة

حسين أ. مرعي، مازن برهان الدين عبد الرحمن، وسام عامر علص
قسم هندسة الانتاج والمعادن / الجامعة التكنولوجية/ بغداد – العراق.

الخلاصة
بحثت هذه الدراسة العلاقة بين سعة القص ومطيلية التقوس لعتبات كابولية خرسانية مسلحة عالية المقاومة تحت تحميل لمرة واحدة, اثناعشر عينة ابعاد مقطعها 200×300 ملم استخدمت في الفحص, تناولت الدراسة تاثير المتغيرات الاتية: نسبة فضاء القص الى العمق الفعال, التباعد بين كانات تسليح القص, مقاومة انضغاط الخرسانة و نسبة التسليح الطولي للشد على تصرف العتبات في منطقة المفصل اللدن مع مراعاة حدوث انماط فشل مختلفة (الانحناء, القص و المشترك), قسمت العينات الى اربع مجاميع حسب متغيرات الدراسة, في كل مجموعة ثلاث عينات تناولت ثلاث قيم من المتغير المدروس تضمن تحول بين انماط الفشل المذكورة. تناولت المجموعة الاولى ثلاث قيم مختلفة من نسبة فضاء القص الى العمق الفعال والتي بزيادتها (من 750 الى 850 ثم بعد ذلك الى 1150 ملم) كان لها تاثير ايجابي على زيادة كل من سعة القص (بنسبة 23% و28%) ومطيلية التقوس (بنسبة 88% و112%) مع حدوث انماط الفشل الثلاثة المذكورة اعلاه والعلاقة بين سعة القص ومطيلية التقوس كانت طردية شبه خطية. المجموعة الثانية تناولت تأثير تباعد كانات القص والتي بزيادتها (من 100 ال 150 ثم الى 300 ملم) ادت الى انحدار في سعة القص (بنسبة 59.7% و 73.5%) ومطيلية التقوس (بنسبة 15.3% و62.5%) والعلاقة المستحصلة بين الاخيرين اظهرت علاقة طردية غير خطية مع انتقال بين انماط الفشل الثلاثة المعروفة. اما المجموعة الثالثة التي بزيادة مقاومة انضغاط خرسانة (من 50.3 الى 55 ثم الى 65 ميغاباسكال) كان تأثيرها سلبي على سعة القص (بنسبة 8.17% و9.13%) بينما ايجابي على مطيلية التقوس (بنسبة 20.17% و153%) مع اظهار انماط الفشل الثلاثة. اما المجموعة الرابعة والاخيرة للعينات والتي كان زيادة نسبة التسليح الطولي للشد هو المتغير الرئيسي فيها حيث كان تأثير هذه الزيادة (من 0.011 الى 0.0151 ثم الى 0.0189) سلبي على كل من سعة القص (بنسبة 34.8% و53.2%) ومطيلية التقوس (بنسبة 55.2% و82.13%) مع حدوث انماط الفشل الثلاثة والعلاقة بينهما طردية خطية.

الكلمات الدالة: عارضة الكابولي؛ ليونة الانحناء؛ الخرسانة عالية القوة؛ قدرة القص؛ طريقة الفشل.

1.INTRODUCTION

High-strength concrete (HSC) has compressive strength over 6000 psi (41 MPa), surpassing ordinary concrete. It meets demands for enduring heavy loads, spanning larger areas, and lasting longer [1]. Materials and mix proportions selection, with additives, including silica fume, fly ash, and superplasticizers, improves high-strength concrete [2]. HSC boosts load-bearing capacity for tall buildings, bridges, and structures. High-strength concrete with a higher elasticity modulus has less deformation under load, which is beneficial for specific structural uses [3]. RC beams resist loads with high-strength concrete, boosting capacity and durability in various applications like high-rise buildings and infrastructure [4]. Shear failure in concrete beams occurs when the beam cannot withstand shear stress, causing diagonal cracks and sudden failure, usually near supports. Stirrups must be sufficient to prevent this brittle failure by maintaining concrete integrity and resisting shear stress [5]. The shear capacity of reinforced concrete (RC) beams is a critical aspect in structural engineering, as it determines the maximum shear force the beam can resist before failure [6]. The beam's dimensions, the properties of the reinforcing concrete and steel, and the load distribution all impact its capacity [7]. Concrete plays a vital role in resisting shear forces due to its natural capacity to endure shear stress. Incorporating steel reinforcement, especially stirrups, improves the beam's capability to withstand extra shear loads [6]. To design and analyze shear capacity in RC beams, several factors should be understood, such as concrete strength, shear span to effective depth ratio, shear reinforcement, beam dimensions, and reinforcement ratios for safety and efficiency. Understanding these factors is crucial for improving shear performance and ensuring structural safety [8]. The plastic hinge zone in reinforced concrete beams allows for significant plastic deformations under high bending forces near supports or high loads, ensuring beam ductility and earthquake resistance [9]. Finding the plastic hinge in RC beams is crucial for predicting bending and deformation locations during loading, necessary for safe structure design, ensuring load-bearing capacity, and enhancing reinforcement effectiveness. Numerous empirical models for plastic hinge length (L_p) are available in Table 1. The plastic hinge length, L_p, is an imaginary length where a consistent plastic curvature is assumed, allowing for evaluating flexural deflection and plastic rotation in RC elements [10].

Table 1 Empirical Models for Plastic Hinge Length [11].

References	Plastic hinge length (L_p)
Baker [12]	$c_0(z/d)^{1/4}d$ (for RC beams and columns)
Sawyer [13]	$0.25d + 0.075z$ (for RC beams)
Corley [14]	$0.5d + 0.2\sqrt{d}(z/d)$ (for RC beams)
Mattock [15]	$0.5d + 0.05z$(for RC beams)
Paulay [16]	$0.08z + 0.022d_bf_y$(for RC beams and columns)
Panagiotakos and Fardis [17]	$0.18z + 0.021d_bf_y$(for RC beams and columns)

where z is the distance from the critical section to the point of contra flexure, d_b is the diameter of longitudinal reinforcement, and c_o is the coefficient related to steel type, axial loading, and concrete strength. A plastic hinge forms faster due to the interaction of maximum moment and shear forces at the same location. However, this process reduces its ability to resist moments and rotate [18]. Plastic hinges often form where moment is high, such as the center of simply supported beams or connection points. These spots can shift due to shear forces [19]. The curvature of reinforced concrete beams is the bending or deformation measure of the beam's longitudinal axis under loads. It is the slope change rate of the deflection curve along the beam's length [20]. The beam's curvature directly affects its shear capacity. When the curvature rises, the beam's shear capacity decreases due to increased curvature, creating a greater need for shear forces in the beam, thus lowering its shear resistance capacity [21-23]. The curvature of RC beams affects their shear capacity and crack patterns, leading to larger cracks and decreased shear capacity. Increased curvature can cause higher tensile strains, leading to diminished shear transfer processes and compromised shear strength, especially with larger curvature [24, 25]. Shear capacity decreases in RC beams with flexural cracks due to altered stress distribution and weakened reinforcement-concrete link. Diagonal crack propagation raises shear failure risk and reduces the beam's resistance to shear force [26]. Understanding RC beam behavior relies on the correlation between moment and curvature. Curvature indicates changes in the angle of the beam's cross-section along its length, dictated by bending moment and material properties. The moment-curvature diagram depicts how beams react to various loads by demonstrating the moment-curvature relationship [27]. Understanding the relationship between moment and curvature is crucial when evaluating the strength of reinforced concrete beams against bending and their resilience to deformation without breaking. When a load is applied to an RC beam, it causes moments and deformation in both the concrete and the reinforcing steel, resulting in curvature. Initially, the beam shows an elastic response, where the curvature increases linearly with the moment. As the load increases, the beam reaches a point where it moves into the inelastic range. In this range, the beam's curvature increases as the steel yields and concrete cracks. Numerous studies (2012) [28, 29] showed high-strength concrete beams failed in shear. Researchers examined HSC beams for shear failure with and without reinforcement. Beams without web reinforcement are brittle; however, shear strength increases with concrete strength. Reinforced beams with stirrups react are less fragile. Arowojolu et al. (2021) [24] showed that, most of the time, higher aspect ratios improve ductility in curves due to shear failures, which occur more frequently as they are more brittle compared to flexural failures caused by smaller ratios. Also, increasing the a/d ratio reduces aggregate interlock's contribution to shear strength, requiring reinforcement adjustments to preserve ductility. Nogueira and Rodrigues (2017) [30] found that shear reinforcement like stirrups boosts concrete's confinement, improving compression resistance and RC beam flexibility. The confinement effect allows beam deformation while preserving strength [31]. In many instances, enhancing the longitudinal reinforcement ratio of RC beams typically enhances their shear capacity. The increased tensile strength of the additional reinforcement enhances its ability to withstand shear stresses, leading to this outcome. Sayhood et al. (2024) [32] found that the compressive strength of concrete significantly impacts the stress capacity of RC beams. Typically, as a material's compressive strength increases, so does its shear strength, enabling it to withstand higher forces before failure. Nguyen et al. (2022) [33] confirmed in Finite-Element Analysis (FEA) studies that increasing concrete's strength improved the load-carrying capacity of RC beams and illuminated stress distribution and failure processes under varying loads. Tamayo and Garcia (2021) [34] indicated that RC beams exhibited increased flexibility with higher compressive strength of concrete. The enhanced strength enables the concrete to withstand more pressure prior to fracturing, thereby allowing for greater deflection and energy absorption.

2.WORKING PROGRAM

2.1.Materials

- **Cement (C):** Ordinary Portland cement Type I was used for casting all specimens. Test results met Iraqi standard IQS No. 5/1984 and ASTM standard C150/CC150M-19a [35].
- **Fine aggregate:** It is commonly referred to as sand, comprises particles smaller than 4.75 mm that can pass through sieve No. 4. The results of the sieve analysis and the physical and chemical tests met the criteria specified in IQS No. 45-1984 and ASTM C778-17 [36].
- **Coarse aggregate:** Crushed gravel, with a maximum size of 10 mm, was utilized as a coarse aggregate. The test results for the coarse aggregate characteristics were assessed according to the criteria specified in IQS No. 45- 1984 and ASTM C33/CC33M-18 [37].
- **Superplasticizer (SP)**: Mega Flow 500 was used as a high-range water-reducing admixture in concrete mixes at a dosage of 1% of the cement amount to decrease the water-cement ratio. It complied with ASTM C-494/C-494M Type F [38].
- **Silica fume:** Silica fume is a 100 times finer pozzolanic substance than cement. It improves concrete permeability and strength in small amounts or as a 10% cement substitute [39]. Chemical composition met ASTM C 1240–05 standards [40].

- **Water:** It was used to cast and cure examples. Its pH level was 7.6, within the range allowed by Iraqi standards (IQS No. 1703, 1992) [41].
- **Steel reinforcement:** Three sizes of reinforcement steel bars were used: 16mm, 12mm, and 6mm. ASTM A615-2018 assessed all these types [42]. The results on reinforcement steel are shown in Table 2.

2.2.Concrete Mixture Proportions

The present study utilized the British Standard approach [43] to formulate and manufacture three concrete mixtures, all classified as high-strength concrete. The desired mixtures comprised strengths of 50.3, 55, and 65 MPa. Table 3 summarizes the specific concrete mixture components employed in the present study.

Table 2 Reinforcement Rebar Characteristics.

Diameters (mm)	Weight (kg/m)	Yield strength (MPa)	Ultimate strength (MPa)
16	1.57	570	600
12	0.88	550	590
6	0.22	510	530

Table 3 Concrete Mixture Components.

Mix designation	Mix components							*f'c* (MPa)	
	Cement (kg/m^3)	Sand (kg/m^3)	Crushed Gravel (kg/m^3)	Silica* fume (kg/m^3)	Water (kg/m^3)	W/C	SP* (kg/m^3)	at 7 days	After 28 days
C1	415	700	1070	0	130	0.313	4.15	36.5	50.3
C2	450	708	1062	0	127	0.282	4.5	38.3	55.0
C3	480	800	1120	48	140	0.265	9.6	47.2	65.0

SP: For superplasticizers, two ratios were used: the first 1% for mixtures C1 and C2, and the second 2% for mixture C3 by weight of cement. Silica fume: used only for the C3 mix with a ratio of 10% of the weight of cement.

2.3.Details of Specimens

The specimens utilized in the present study as a cantilever beam were subjected to a concentrated point load at the end, measuring (300×200) mm in section size, 2350 mm in total length, with a cantilever length of 1250 mm. A rigid column of 700 mm height was placed in the middle of the specimens to enhance joint stiffness (as shown in Fig. 1(b) and Fig. 2). This cantilever specimen aims to replicate the behavior of continuous reinforced concrete beams with a length of 5 m affected by two concentrated point loads (Fig. 1(a)). Both shear and flexural stresses coincide within the plastic hinge region. Numerous researchers have adopted this method to study failures near and at joints under dynamic and seismic loads by removing a segment of the continuous beam at the inflection point [44-49], as illustrated in Fig. 1(a) and (b). The study comprises twelve samples, segmented into four groups according to the variables analyzed: shear span to effective depth ratio (a/d), transverse reinforcement, concrete compressive strength, and longitudinal reinforcement. Details of the longitudinal and transverse reinforcement for the samples in the present study are outlined in Table 4. It is crucial to highlight that each group exhibited varying failure modes based on the parameter values, as specified by the ACI 318R-19 [50]. Figure 3 shows all details of the reinforcement (flexural and shear), shear span values, the sample names of each group, and the key parameters concerning shear strength. In group A, the shear span to effective depth (a/d) was specified by three values: 4.32, 3.195, and 2.82. Group B shows different stirrup spacing options, i.e., 100 mm, 150 mm, and 300 mm. All specimens were reinforced outside the plastic hinge region with stirrup reinforcement, placed 50 mm apart to prevent failure outside it (as shown in Fig. 3). Group C presents varying compressive strengths of concrete, i.e., 50.3 MPa, 55 MPa, and 65 MPa. Lastly, Group D showcases various tension longitudinal reinforcement setups, i.e., #3Φ16mm (0.0113), #4Φ16mm (0.0151), and #5Φ16 mm (0.0189).

2.4.Mixing and Casting Procedure

The wooden models used in this study were all 2.35 m long and were of uniform size. Once the mold was cleaned and oiled inside, steel reinforcement bars were inserted after securing the components. An electric tilting rotary mixer, with a capacity of 0.19 m3, was utilized to blend the concrete. Following the specified proportions, the coarse aggregate, cement, and silica fume were successively added after measuring and recording the required materials. The mixing speed of the electric tilting rotary mixer was set to approximately 15 rpm to ensure even distribution of the silica fume. Subsequently, the superplasticizer was mixed with water and allowed to rest for 35 seconds. After mixing for about seven minutes, the fine aggregates, remaining superplasticizers, and water were introduced. Typically, it took around 10 minutes to mix one batch to the desired consistency. Procedures for mixtures containing no silica fume mirror those without it. After mixing materials, the mixture was placed in wooden molds in layers (see Fig. 4) and then consolidated using a vibrator. The upper surface was polished, and 6 cylinders for tests, 3 for each strength type, were made [51]. Also, three prisms for rupture tests were made [52]. Additionally, 3 cubes for control were included in each batch [53]. The samples were removed from the molds, wrapped in blankets, and soaked in tap water for 28 days, as shown in Fig. 4. This method simulates the treatment of structural parts without submerging them in water, instead using a spraying technique. After 28 days, the covers were removed. Models were covered in white emulsion to highlight cracks. Then, shear strength testing was performed.

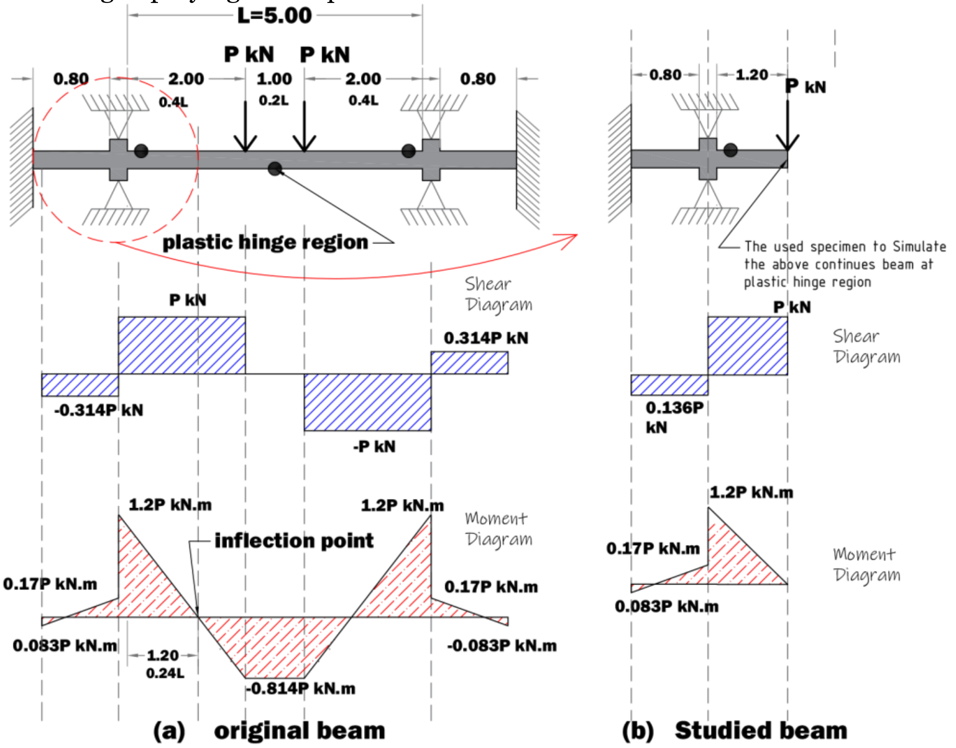

Fig. 1 (a) The Original Beam, (b) Experimental Specimen Used.

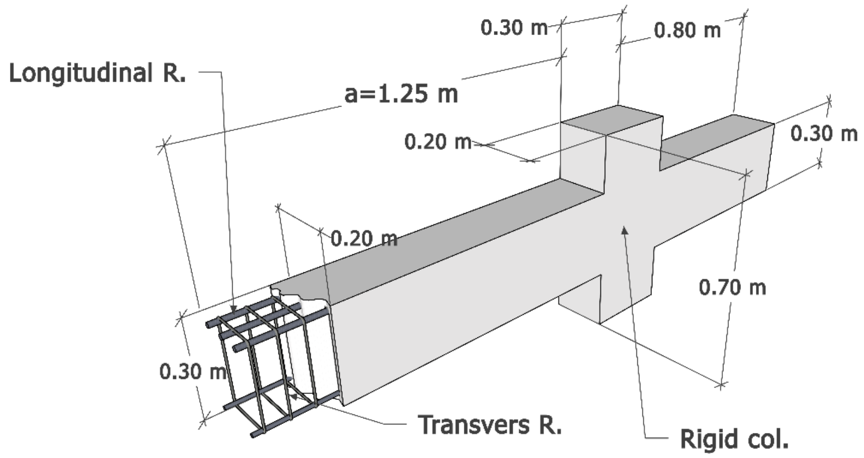

Fig. 2 Specimen Dimensions.

Table 4 Details of Specimens and Material Properties.

Group	Specimen Notation	Shear Span	Comp. Strength	Longitudinal Tensile Reinforcement		Transvers Reinforcement	
		a (mm)	f'_c (MPa)	#Long. Steel	f_y (MPa)	Stirrups spacing	f_{vy} (MPa)
A	Aa75*	750	65	3Ø16	570	300	530
	Aa85	850	65	3Ø16	570	300	530
	Aa115	1150	65	3Ø16	570	300	530
B	Bs100*	750	65	3Ø16	570	100	530
	Bs150	750	65	3Ø16	570	150	530
	Bs300	750	65	3Ø16	570	300	530
C	Cc1*	850	50.3	3Ø16	570	300	530
	Cc2	850	55.0	3Ø16	570	300	530
	Cc3	850	65.0	3Ø16	570	300	530
D	Bp3*	850	65	3Ø16	570	150	530
	Bp4	850	65	4Ø16	570	150	530
	Bp5	850	65	5Ø16	570	150	530

*Note: These are control samples for each group. All specimens have an effective depth (d) of 266 mm.

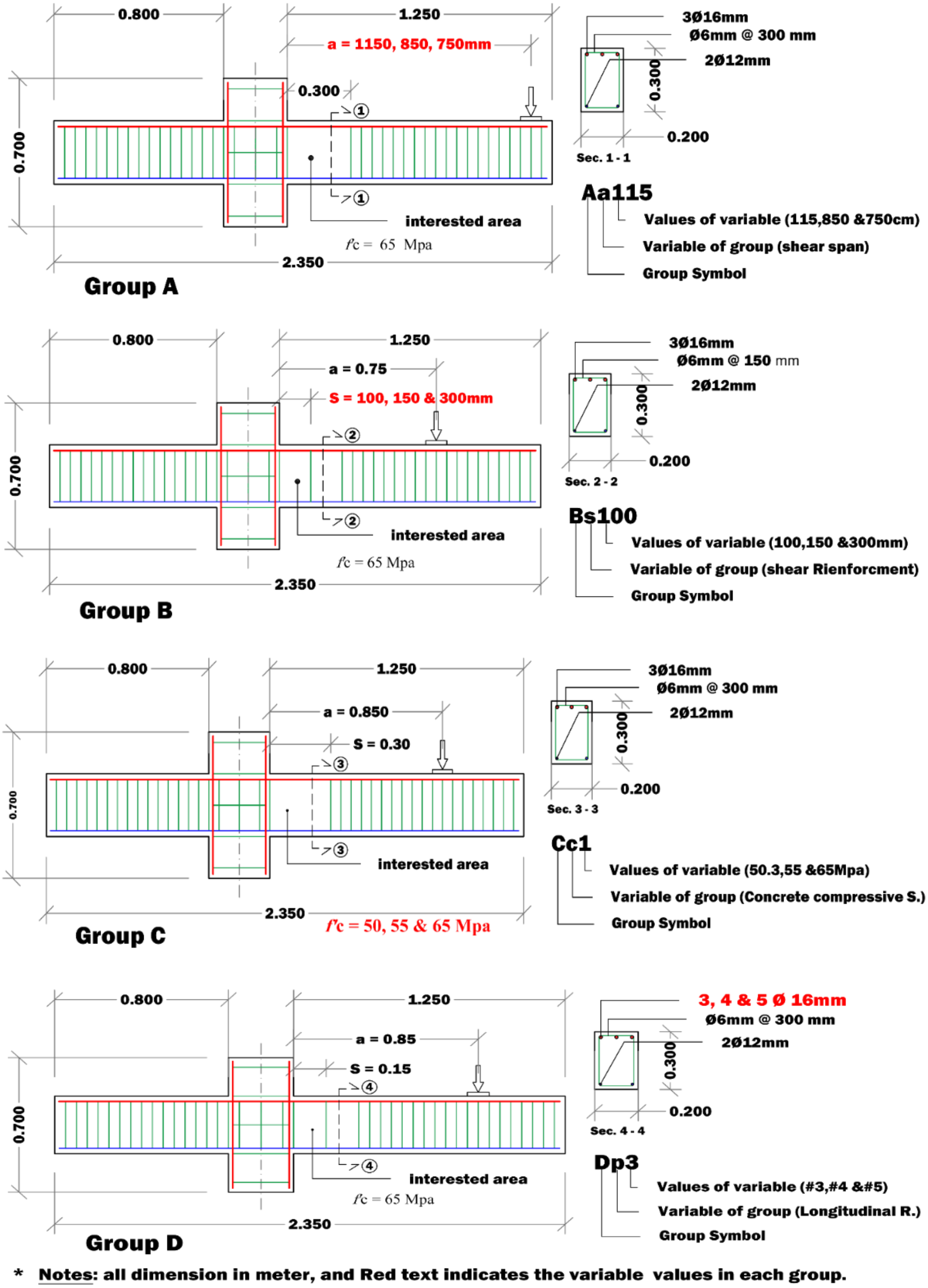

Fig. 3 Geometry and Reinforcement of Specimens, All Dimensions in (m).

Casting of beams with mixture. Humidity-treated specimens.

Fig. 4 Concrete Mixing and Casting Process.

2.5.Specimen Tests

After preparing the cantilever samples for examination, the sample placed in the testing machine with horizontal balancing achieved using a bubble leveling device (Fig. 5). The sensors and equipment were installed in the following manner: Two specially designed steel collars were securely fastened to the sample's body and housed two LVDTs positioned above and below the target area (for curvature measurement). Additionally, a third LVDT positioned at the cantilever sample's end was used solely for measuring vertical deflection, as shown in Fig. 6. Two types of strain gauges for flexural and shear steel were also used (Fig. 7 and Table 5). A data logger was utilized to record and store data from all sensors, i.e., LVDTs, steel strain gauges, and load cell, and was connected to a computer through a dedicated program (as shown in to Fig. 8). A concentrated load was applied at a loading speed of 1 mm/min from the jack using the electric-hydraulic pressure system with a 200-ton capacity. A camera and visual monitoring were employed to detect cracks in the target region and the sequence of their formation to determine the load value at each crack, see Fig. 9. The load will be consistently applied until yielding results in the final failure.

Table 5 Strain Gauge Details.

Types	Strain G. Length	Resistance	Gauge Factor	Setting Location
BMB120-3AA-P1000-D	6 mm	120±0.3Ω	2.0±1%	Steel bar
BMB120-80AA-P1000-D	90 mm	120±0.3Ω	2.11±1%	Concrete surface

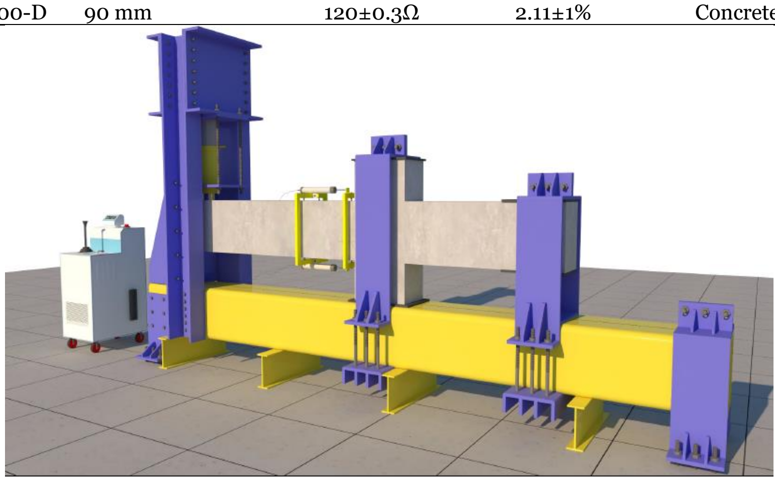

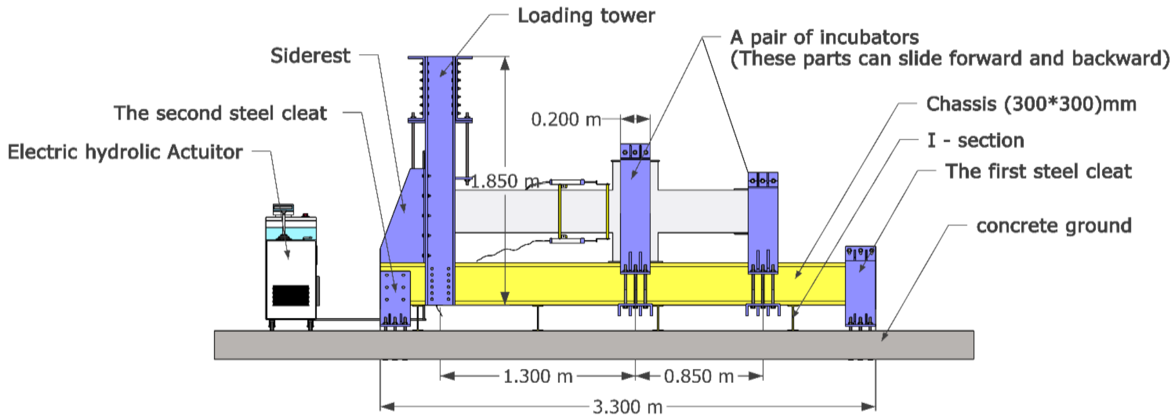

Fig. 5 Diagram of Beams Installed with Device.

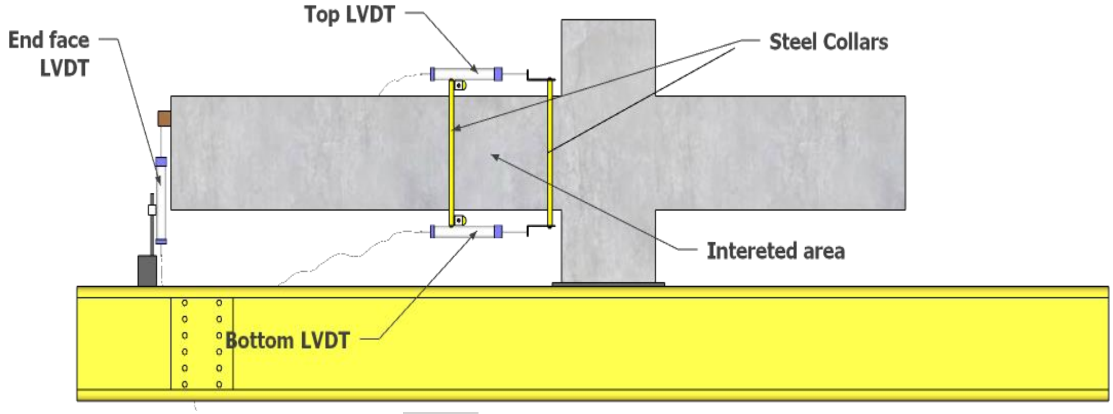

Fig. 6 LVDTs Installation.

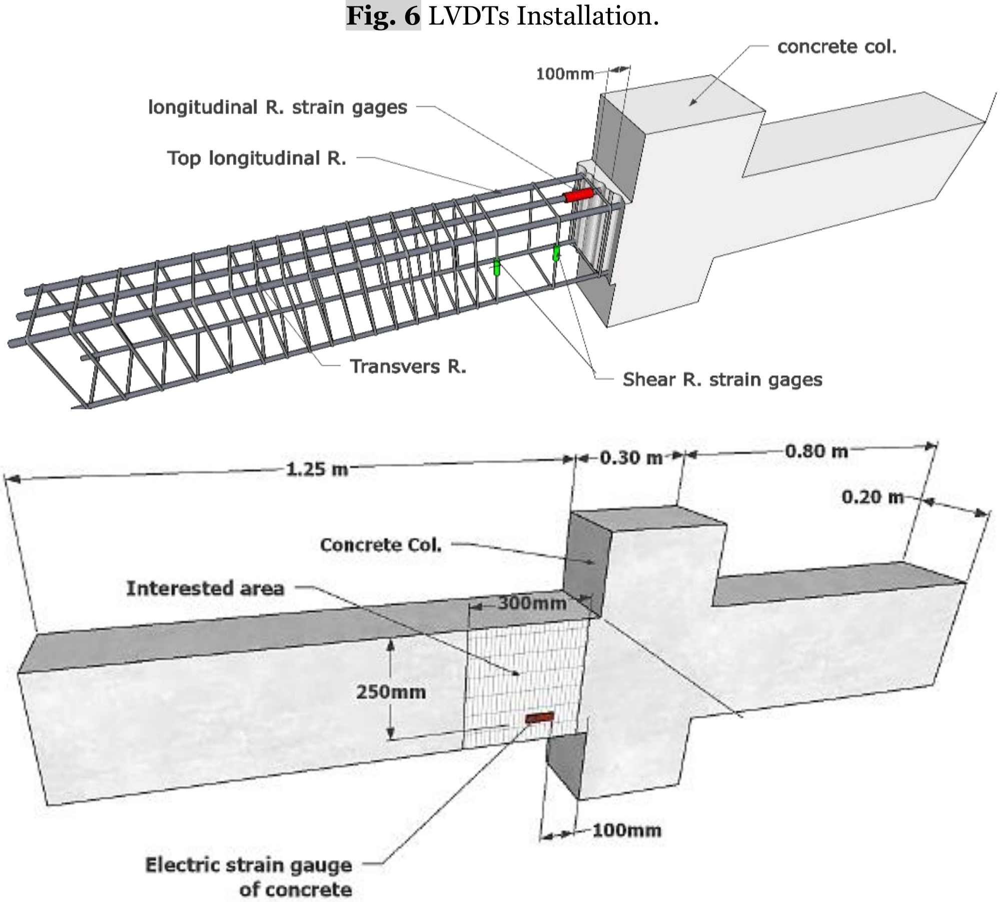

Fig. 7 All Strain Gauge Positions.

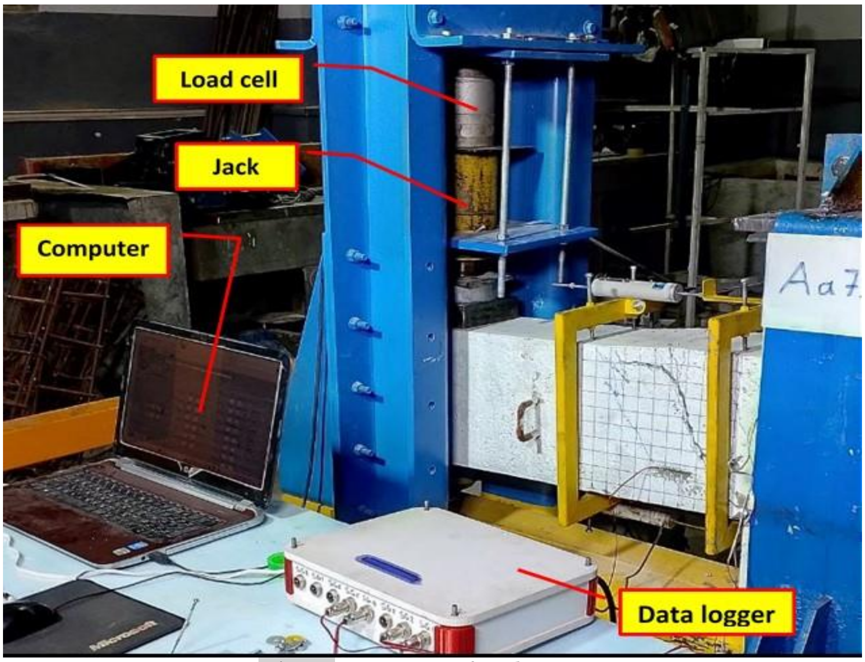

Fig. 8 Preparing for the Test.

Fig. 9 Loading and Monitoring System.

3.RESULTS AND DISCUSSIONS

3.1.General Behavior and Crack Development

The present study grouped the specimens into four categories based on the variables they handled. Each group comprised three beams, with variable values changing, leading to shifts in failure mode, such as shear, combined, and flexural mode, or vice versa, as per the ACI code design equations. Variations in the failure mechanisms, shapes, formation processes, and crack distribution were observed in the tested beams within each group. Initially, no cracks were seen during early loading stages. Later, flexure and shear cracks appeared and were carefully recorded as the load increased gradually, leading to eventual failure within the specified region of interest in each beam specimen located 300 mm from the column face (where the maximum moment, maximum shear, and plastic hinge area are situated). The flexural cracks first appeared in the test beams' interest area. More cracks developed as the load rose, with one growing significantly, eventually leading to the main crack signifying flexural failure, despite diagonal cracks, seen in Aa115, Bs100, Cc3, and Dp3. In another scenario, the flexural cracks' growth rate slowed as the load increased. This behavior coincided with the emergence of diagonal splitting cracks that expanded and widened with increasing load. Ultimately, these cracks intersect with cracks resulting from flexural stresses in the region and propagate downward, forming a pattern of cracks indicating a combined failure mode, which is seen in the Aa85, Bs150, Cc2, and Dp4 samples. When shear failure was the main factor, the load was near its maximum, and a main inclined shear crack would widen, becoming a diagonal crack between the load and support point. The splitting near the support was caused by its downward force and the tensile steel reinforcement, leading to a failure mode that resembles shear failure more closely, as seen in Aa75, Bs300, Cc1, and Dp5. Determining the failure mode based on the cracks' shape and locations may not provide conclusive evidence. The final decision on determining the failure mode depends on the yielding of the reinforcement used in shear or bending [54]. Figures 10 to 13 display the crack appearance for each group. The varying (a/d) ratio in group A, with values of 2.82, 3.19, and 4.32, influenced crack development. Increasing the (a/d) ratio led to more flexural cracks with a decrease in shear cracks, intensifying bending stresses and moments in the area, as shown in Fig. 10. A lower a/d ratio below 2.5 results in more shear stresses and diagonal shear cracks, while higher ratios led to vertical flexural cracks [24, 46]. The study examined how different stirrup spacing values of 100 mm, 150 mm, and 300 mm affected shear reinforcement in Group B. The results showed that greater shear reinforcement caused more noticeable bending cracks and enhanced bending response, as illustrated in Fig. 11. Increased stirrup spacing increased the beam's shear capacity, supported the longitudinal reinforcement, and stiffened the beam to minimize flexural cracks, ultimately improving structural integrity and serviceability [55]. In group C, which focused on studying the compressive strength of concrete, it was noted that higher compression values, i.e., 50.3, 55, and 65 MPa, led to a decrease in both bending and shear crack occurrences (as shown in Fig. 12). Concrete with higher strength resists flexural and shear cracking in beams better. Increased strength delays crack formation and reduces its width due to improved stiffness and carrying capacity [55]. Group D analyzed three percentages, i.e., 0.011, 0.0151, and 0.0189, and focused on the impact of the longitudinal reinforcement ratio. Higher reinforcement ratios decreased bending cracks but increased shear crack width, affecting bending response, as shown in Fig. 13. Increasing reinforcement enhanced beam flexibility and strength, delaying crack formation with improved stress distribution for better structural integrity [56].

3.2. Ultimate and Cracking Load

Table 6 shows ultimate load, cracking load, deflection, and failure mode for flexural and shear tested beams. Deflection values were smaller when the failure mode was shear, with half of the beams failing in flexural. This result aligns with many earlier studies [57] and [58] that emphasize the sudden and dangerous nature of this type of failure, which often happens without adequate warning. Conversely, higher deflection values were observed in cases of combined and flexural failure modes.

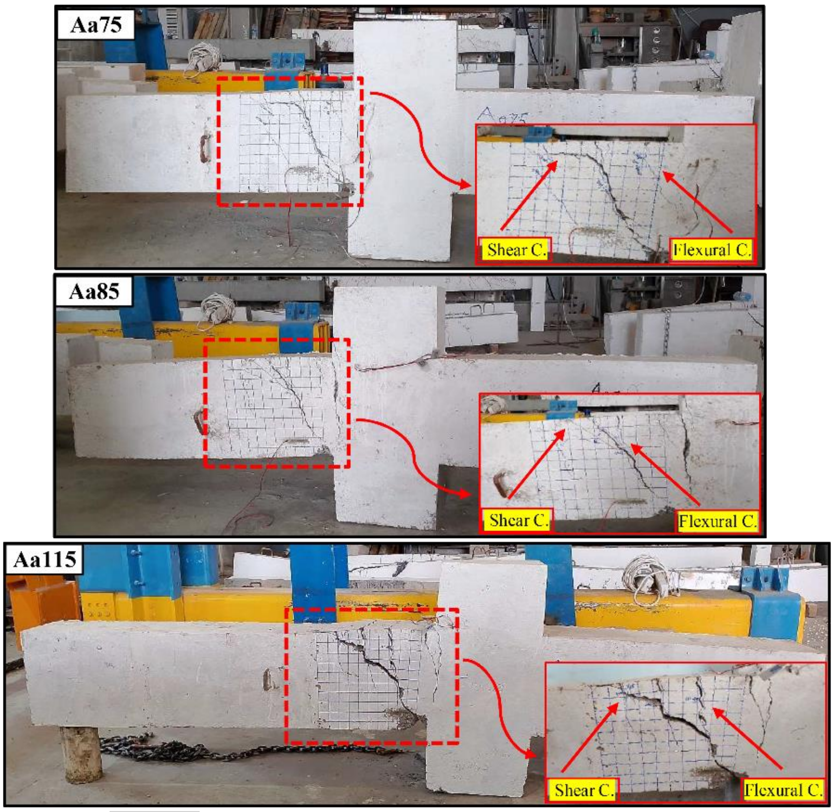

Fig. 10 Final Crack Patterns of Group (A) Specimens.

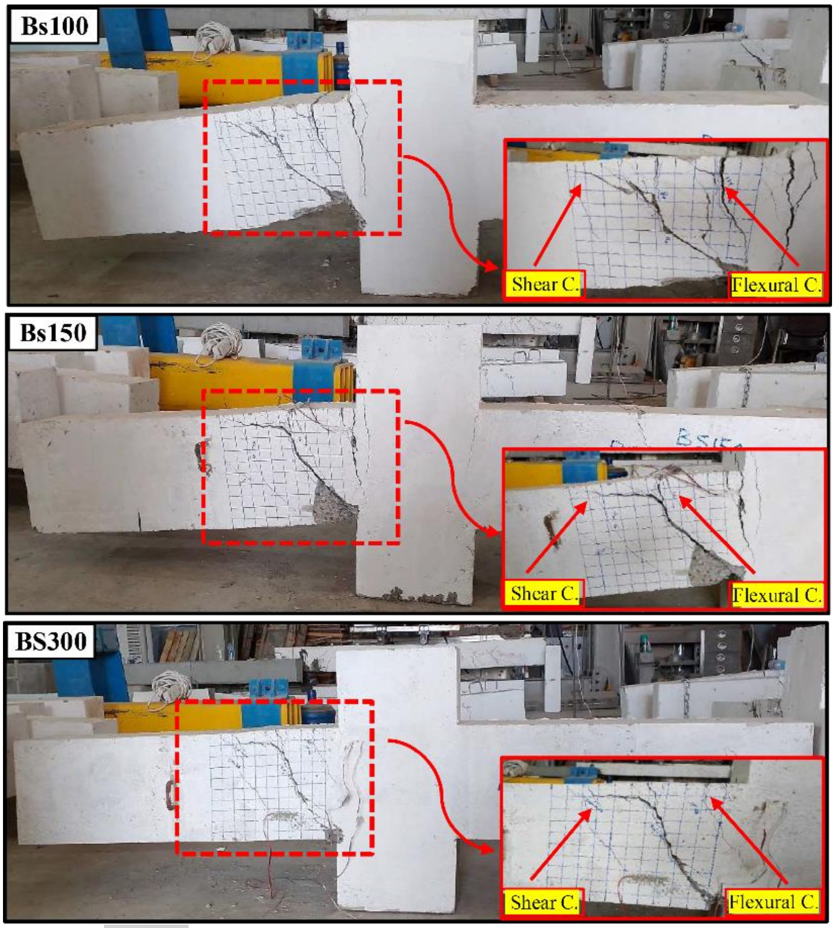

Fig. 11 Final Crack Patterns of Group (B) Specimens.

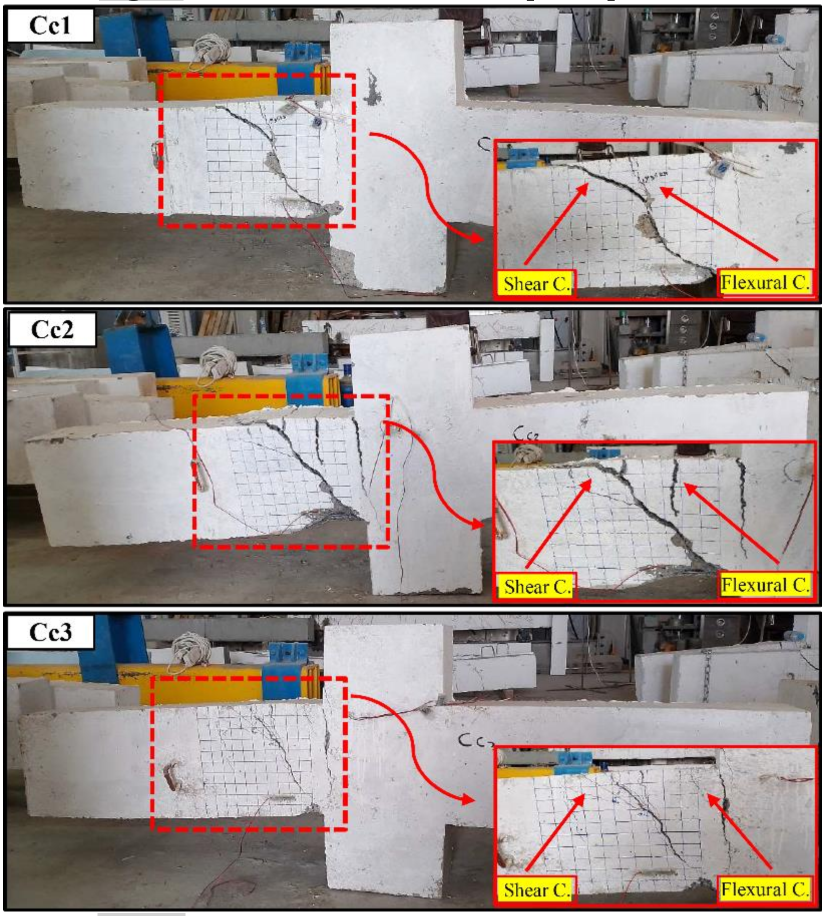

Fig. 12 Final Crack Patterns of Group (C) Specimens.

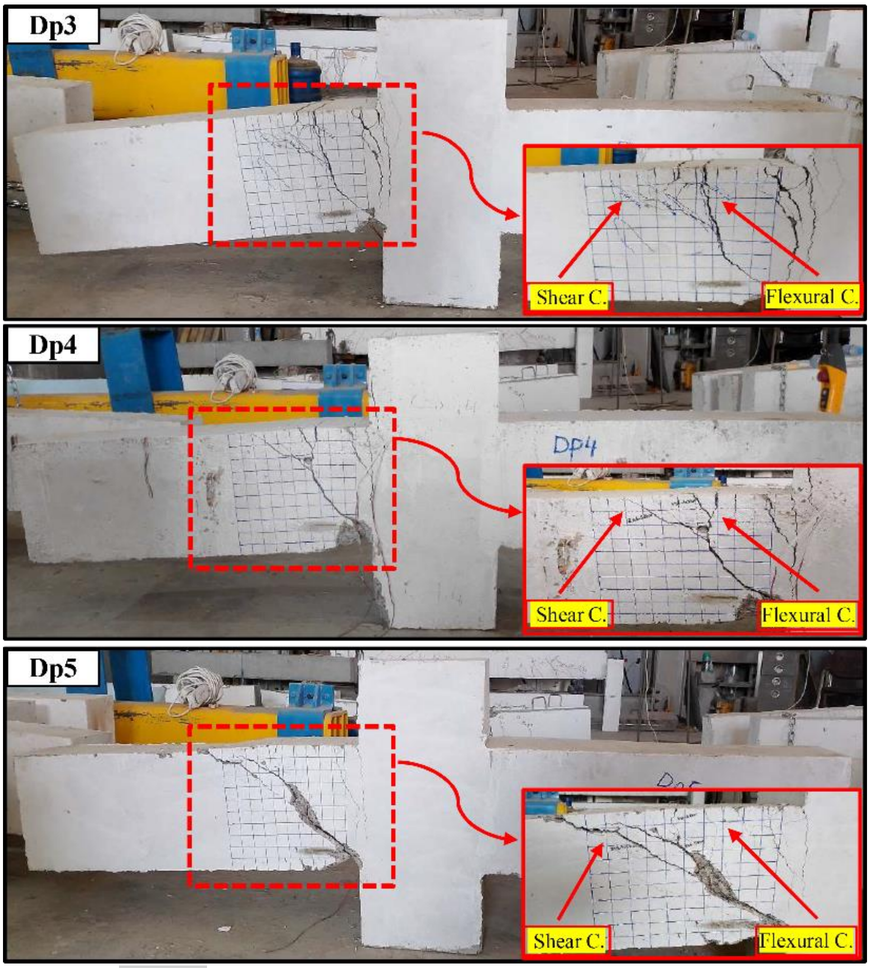

Fig. 13 Final Crack Patterns of Group (D) Specimens.

It was found that bending cracks were closer to the joint than shear cracks, occurring within distances of 50 to 150 mm, while shear cracks form at distances greater than 250 mm (as shown in Figs. 10 to 13). Many studies have confirmed that bending cracks occur in the plastic hinge area. In Table 1, various equations were suggested to determine the extent of this joint.

Table 6 Test Results for Beam Specimens.

Group Sy.	Spec.	P_{fl} (kN)	δ_{fl} (mm)	D_{fl} (mm)	P_{sh} (kN)	δ_{sh} (mm)	D_{sh} (mm)	P_u (kN)	δ_u (mm)	Observed Failure Mode
A	Aa75*	40.3	3.5	50	44	4.1	210	140.1	34.3	Shear failure
	Aa85	40	6.9	120	50	8.9	280	127.0	62.4	Combined failure
	Aa115	25	6.4	125	65	17.2	285	98.9	73.22	Flexural failure
B	Bs100*	34	3.7	210	45	5.3	300	139.7	47.5	Flexural failure
	Bs150	35	5.4	160	50	7.6	285	129.2	67.8	Combined failure
	Bs300	37.1	5.8	90	41	5.2	280	126.8	37.5	Shear failure
C	Cc1*	32	3.0	120	55	6.4	270	109.0	39	Shear failure
	Cc2	36	5.9	150	95	16.7	230	117.7	35.4	Combined failure
	Cc3	39.6	6.3	117	50	9.2	290	126.5	61	Flexural failure
D	Dp3*	26	5.5	130	44	8.9	290	120.0	73.7	Flexural failure
	Dp4	43	4.3	130	48	5.0	300	163.2	69	Combined failure
	Dp5	38	7.2	185	53	9.8	290	173.5	43.5	Shear failure

* These are the control samples for each group.

3.3.Curvature Assessment

Experimental tests on reinforced concrete measured support reactions, displacements, curvatures, and strains to evaluate structural behavior. Curvature (ϕ) measures deformation in a cross-section, defined as the rotation angle per unit length during bending [59]. The derivative of the tangent's inclination to arc length can be determined (Fig. 14).

$$\textbf{Curvature: } \phi = \frac{d\theta}{dy} = \frac{d^2y}{dx^2} = \frac{1}{\rho} \quad (1)$$

$$\phi = \frac{M}{EI} \quad (2)$$

Where *EI* denotes the flexural stiffness. Aules et al. (2019) [60] used an experimental approach to evaluate the curvature, as shown in Fig. 15. This method calculates the curvature of all samples throughout the loading range. Two LVDTs were securely attached in place. The first one was placed on the top surface of the target area, 300 mm away from the column face, and extended towards the loading point with a 30 mm gap to prevent slip from impacting the LVDT measurements. The second LVDT was positioned at the bottom of the target area. Figure 16 shows where the LVDT was placed and its dimensions. The curvature was determined using Eq. (3):

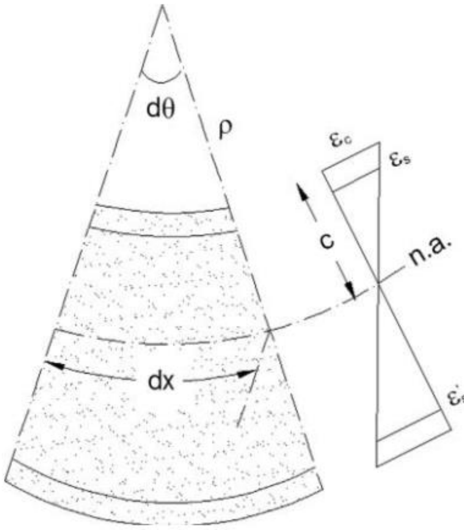

Fig. 14 Moment Curvature Relationship.

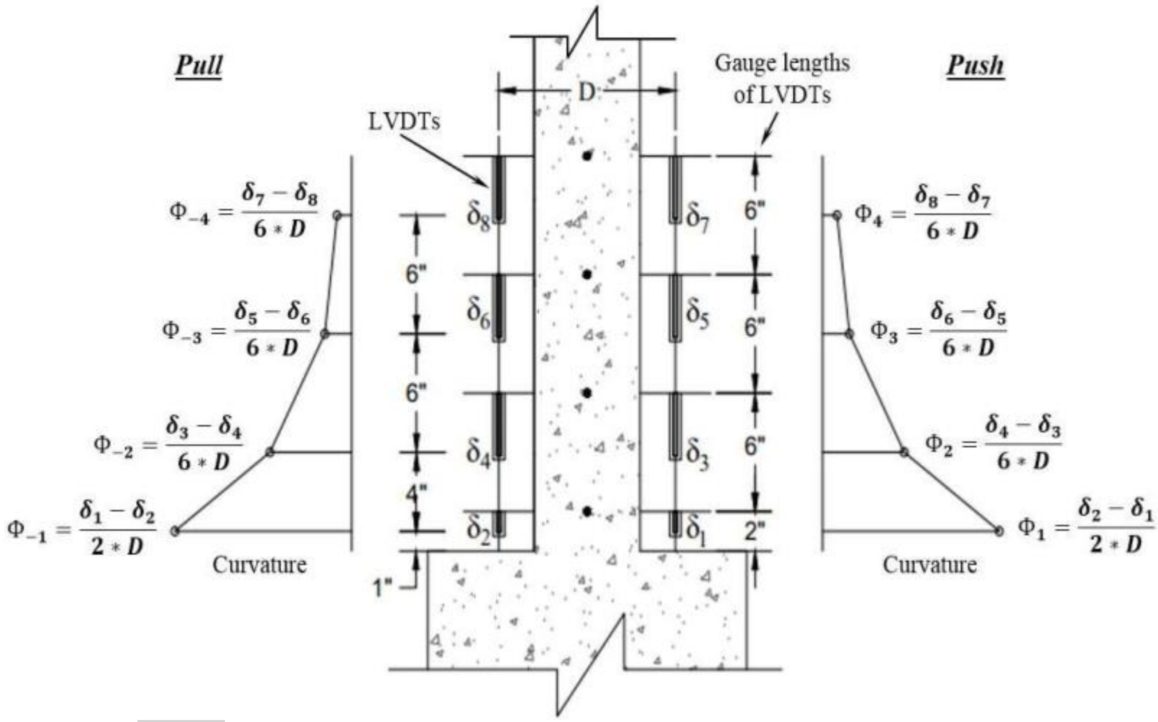

Fig. 15 LVDTs Arrangement and Curvature Calculation Mechanism [60].

$$\Phi = \frac{/\delta_{top}/+/\delta_{bott}/}{300 * d'} \quad (3)$$

where δ_{top} is the horizontal displacement of the LVDT at the top, δ_{bott} is the horizontal displacement of the LVDT at the bottom, and d' is the spacing between LVDTs. Table 7 lists curvature values for beam specimens tested at first crack load for flexural, first crack load for shear, and ultimate load. When analyzing beam curvature values, altering study variables indirectly impacts curvature; however, it influences failure mode, consequently affecting curvature values. Studying beams that fail from flexural or combined stress showed higher curvature values than shear failure beams. This trend was consistent across all categories and factors examined, indicating that the occurrence, number, and width of flexural cracks in the region contributed to the beams' increased curvature.

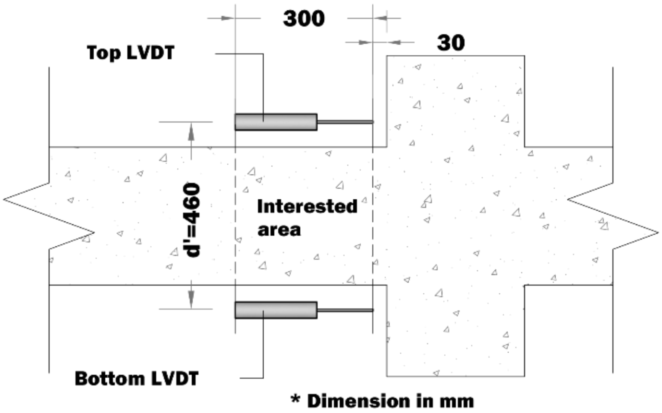

Fig. 16 LVDT's Location for Curvature Assessment.

3.4.Moment–Curvature Relationship

Understanding this relationship allows engineers to anticipate how reinforced concrete beams will react under various loads and create buildings that are safe and cost-effective [61]. Wight and MacGregor (2016) [62] emphasized the importance of the moment-curvature relationship in RC structure design and analysis.

This relationship is crucial for maintaining structural integrity against seismic and dynamic loads. The research shows how variables impact the relationship in the concrete beams examined.

Table 7 Curvature Values at Various Loading Durations.

Groups Sy.	Spec.	P_{fl} (kN)	ϕ_{fl}* *10^{-3} (rad/mm)	P_{sh} (kN)	ϕ_{sh}* *10^{-3} (rad/mm)	P_u (kN)	ϕ_u* *10^{-3} (rad/mm)	Observed Failure Mode
	Aa75*	40.3	0.001998	44	0.003124	140.1	0.049602	Shear failure
A	Aa85	40	0.002906	50	0.004570	127.0	0.088229	Combined failure
	Aa115	25	0.002764	65	0.009209	100.4	0.088731	Flexural failure
	Bs100*	34	0.001795	45	0.003046	140.1	0.057645	Flexural failure
B	Bs150	35	0.002371	50	0.003701	129.2	0.093087	Combined failure
	Bs300	37.1	0.001664	41	0.002135	126.8	0.014691	Shear failure
	Cc1*	32	0.002561	55	0.006281	109.0	0.031459	Shear failure
C	Cc2	36	0.002201	53	0.004716	117.7	0.034786	Combined failure
	Cc3	39.6	0.002850	50	0.004475	125.0	0.052758	Flexural failure
	Dp3*	26	0.001238	44	0.003281	120.0	0.128810	Flexural failure
D	Dp4	43	0.003065	48	0.003753	163.2	0.073031	Combined failure
	Dp5	38	0.002384	53	0.003891	173.5	0.035048	Shear failure

* These are the control samples for each group.

- ***a/d Ratio Effecting***
  The variable in RC beams classified as Group A was studied using three values of a/d ratio: 2.7, 3.14, and 4.63. Figure 17 (a) shows the effect of variation of a/d ratio values on the Curvature-Moment relationship. The group A beams behaved similarly, with varying levels of plastic deformation as the a/d ratio increased. Beam Aa115 deviated due to issues with steel collars supporting LVDTs, caused by concrete breaking. Constraint process ended, freeing her.
- ***Hear Reinforcement Effecting (Stirrups Spacing)***
  Figure 17 (b) shows the effect of variation of stirrups spacing on the Curvature-Moment relationship in Group B, specifically looking at how shear reinforcement affects them at stirrup spacing of 100, 150, and 300 mm. The beams in this Group showed different levels of plastic deformations with an increase in shear reinforcement. This variation is due to the change in final failure modes mentioned previously.
- ***Concrete Compressive Strength Effecting***
  Figure 17 (c) shows the effect of variation of concrete compressive strength on the Curvature-Moment relationship of group C specimens. The group studied three specific values: 50.5, 55, and 65 MPa for this aspect. The beams in Group C showed similarities to the earlier groups, as they demonstrated increased strength with higher variable amounts. Nonetheless, they exhibited greater plastic deformation.
- ***lexural Reinforcement Effecting***
  Figure 17 (d) shows the effect of flexural reinforcement ratios (top reinforcement) on the Curvature-Moment relationship of Group D specimens. Three ratios were used: 0.01134 (3Ø16mm), 0.0151 (4Ø16mm), and 0.01888 (5Ø16mm) MPa.

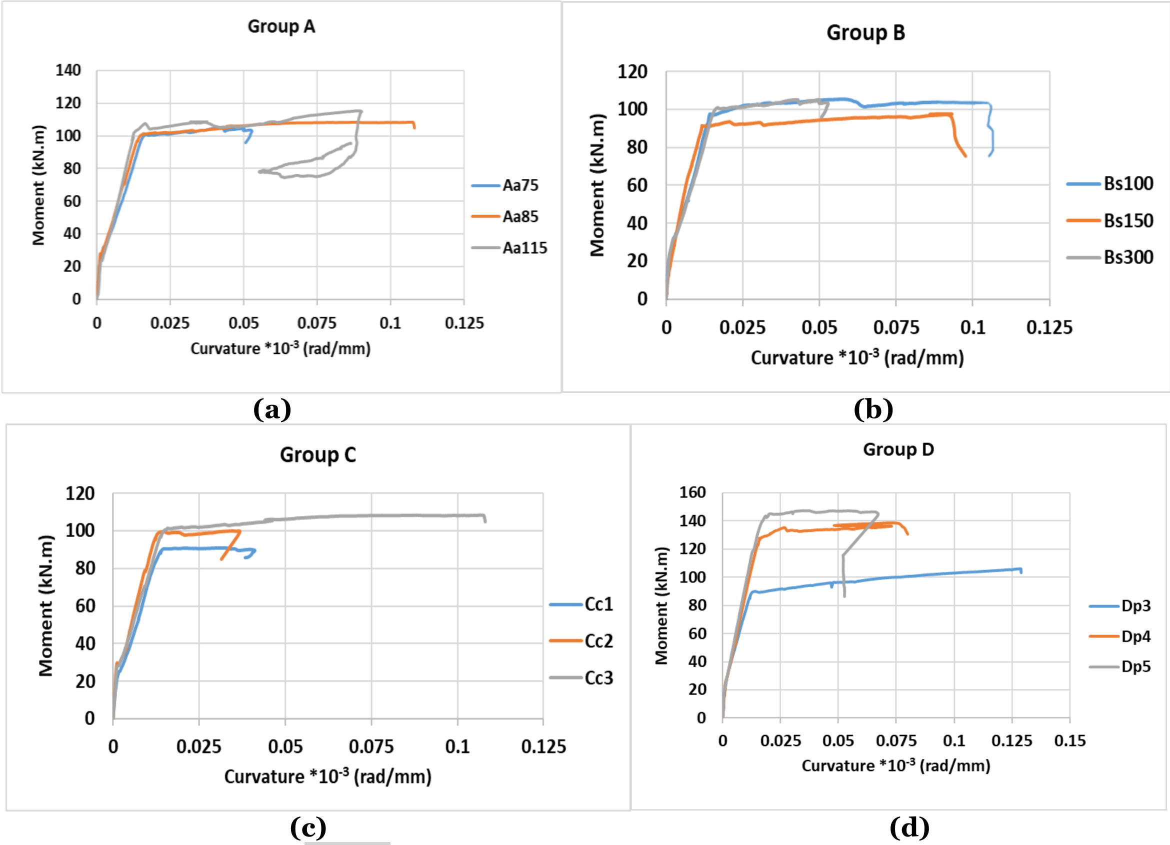

Fig. 17 Moment-Curvature R. of All Specimens.

The beams of Group B exhibited different behavior compared to those of earlier groups. Although they could bear more weight because of added flexural reinforcement, there was a decrease in plastic deformation.

3.5.Shear Capacity

Sometimes, researchers use the terms "shear capacity" and "shear strength" interchangeably in the context of reinforced concrete (RC) beams. Nonetheless, these terms have distinct and precise definitions in structural engineering. In RC beams, shear strength is the maximum stress a material can handle without breaking. It involves the property affecting its ability to resist shear forces and prevent failure. The shear capacity is the maximum shear force a structural element can handle before failing due to shearing. It includes the natural strength of materials and safety measures for load endurance [63]. The capacity of a beam to resist shear forces is influenced by various elements, such as its shape, size, and the type, besides quantity of concrete and reinforcement materials, the use of shear reinforcement, and the way it is loaded and supported. Simply, shear strength measures how well a material can withstand shear stress, while shear capacity indicates the actual shear force that a beam can support, accounting for design factors and safety margins. The two main shear capacity elements of reinforced concrete (RC) beams are:

Concrete Contribution (Vc): Shear strength from the concrete itself is influenced by factors, including compressive strength, cross-section dimensions, and stress distribution. Codes provide equations for concrete shear capacity calculation, e.g., the ACI 318-19 code formula for nominal shear strength calculation [50].

$$V_c = 0.17\sqrt{f'c}bd \qquad (4)$$

The predicted shear in ACI 318-19 could be inaccurately high, so researchers proposed new equations to study shear resistance in concrete. They consider parameters, including joint flexibility, aggregate roughness, and the usual factors of strength and size. Rodrigues et al. (2010) [64] proposed a design Eq. (5) to estimate the shear capacity of concrete (V_c). The equation considers factors, including effective depth, shear span, flexural reinforcement ratio, yield strength of flexural steel, concrete compressive strength, rotation value, and aggregate size, based on the principles of the critical shear-crack theory (*CSCT*) [64].

$$\frac{V_{cr}}{b \cdot d\sqrt{f'_c}} = \frac{1}{6} \cdot \frac{1}{1 + 2 \cdot \frac{\theta t \cdot d}{16 + d_g}} \qquad (5)$$

The total rotation of the beam being analyzed comprises the initial rotation due to elastic deformation and the extra rotation from inelastic deformation, which includes the creation of plastic hinges, as described in the equation provided by Kheyroddin and Naderpour (2007) [65].

$$\theta_{\text{total}} = \theta_{\text{elastic}} + \theta_{\text{inelastic}} \qquad (6)$$

The elastic rotation at the free end ($\theta_{elastic}$) is calculated using the vertical displacement (δ) measured by LVDTs and the length of the cantilever (L) [66]:

$$\theta_{elastic} = \frac{\delta}{L} \quad (7)$$

While the inelastic rotation based on the plastic hinge length and curvature change [65] is calculated

$$\theta_{inelastic} = L_p(\phi_u - \phi_y) \quad (8)$$

Shear Reinforcement Contribution (Vs): Vs refers to the shear strength provided by the shear reinforcement, typically in the form of stirrups or bent-up bars. Shear reinforcement is crucial for enhancing the shear capacity and controlling shear cracks [50]. The force carried is calculated by the stirrups, and the recorded strain (ϵ_s) is converted to stress (σ_s) using the material's stress-strain relationship. For steel, this relationship is typically linear up to the yield point and can be expressed using Hooke's Law:

$$\sigma_s = E_s \cdot \epsilon_s \quad (9)$$

where E_s is the modulus of elasticity of the steel. The shear strength provided by shear reinforcement, as the sum of the tensile force of all the stirrups (V_{sw}) crossed by the critical shear cracking (*CSC*) [67], was:

$$V_{sw} = \sum \sigma_{sw} \cdot A_{sw} \quad (10)$$

The above equation provides the value of the transverse steel's participation in resisting applied shear stresses, while the residual shear strength is required. This value can be found by subtracting the value of the design nominal shear strength (V_{sn}) calculated from Eq. (11). "This expression is used to determine structural elements' shear strength of steel in design codes ACI 318-19" [50] from the steel's participation in Eq. 10, as expressed in Eq. (12).

$$V_{sn} = \frac{A_v f_y d}{s} \quad (11)$$

$$V_{sr} = V_{Sn} - V_{sw} \quad (12)$$

where f_y is the yield strength of shear reinforcement, d is the effective depth of the member, s is the distance between stirrups along the member length, and V_{sr} is the residual capacity of shear steel. Finally, the main goal of this study is to combine the residual shear capacity of the concrete and the transverse reinforcement to determine the total residual shear capacity (V_{tr}) of the structural element (beam).

$$V_{tr} = V_{sr} + V_{cr} \quad (13)$$

Table 8 presents the shear capacity values for concrete and steel individually and combined for all beams analyzed in this study. Figure 18 shows the variation of shear capacity values between beams in each group. Where V_{cr} is the residual shear capacity of concrete, V_{Sw} is the contribution shear strength of stirrups, V_{Sn} is the nominal shear capacity of stirrups, V_{Sr} is the residual shear capacity of stirrups, and V_{tr} is the total residual shear capacity of the beam. When examining the shear capacity values of concrete, particularly in the fourth column of Table 8, it is evident that these values are almost zero in all beams examined. This result indicates that the concrete's ability to withstand shear stresses has been exhausted. It should be noted that in some beams, failure due to bending was more prominent.

Table 8 Shear Capacity Values for All Beams.

Speci.	P_u (kN)	θ_t (rad)	V_{cr} (kN)	V_{Sw} (kN)	V_{Sn} (kN)	V_{Sr} (kN)	V_{tr} (kN)
Aa75*	140.3	0.054	0.093	12.42	28.57	16.14	16.23
Aa85	127.4	0.083	0.061	7.84	28.57	19.90	19.96
Aa115	98.9	0.079	0.064	8.66	28.57	20.73	20.79
BS100*	140.1	0.076	0.066	23.27	85.70	62.42	62.49
BS150	129.2	0.092	0.055	32.04	57.13	25.09	25.14
BS300	126.8	0.055	0.091	12.15	28.57	16.42	16.51
Cc1*	107.0	0.085	0.052	5.74	28.57	22.82	22.88
Cc2	117.7	0.076	0.061	7.62	28.57	20.94	21.01
Cc3	126.5	0.093	0.054	7.83	28.57	20.74	20.79
Dp3*	120.0	0.102	0.050	7.68	57.13	49.45	49.50
Dp4	162.0	0.087	0.058	24.92	57.13	32.21	32.27
Dp5	173.5	0.088	0.057	34.01	57.13	23.12	23.17

* These are the control samples for each group.

This result could be explained by the researcher's suggestion that shear failures occur following the yielding of flexural reinforcement, causing the crack width to widen with rotations, ultimately weakening the mechanisms carrying shear forces. Consequently, the rotation capacity of plastic hinges increased as shear forces decreased [64]. The failure of the transverse steel is crucial in determining how it helps resist the shear stresses. If the main way it fails is due to shear, the steel's ability to withstand shear decreases significantly. However, if the main failure mode is flexural, the decrease in shear resistance is less pronounced. Furthermore, adding more shear reinforcement in beams can slow down the reduction of concrete shear capacity by limiting the formation, spreading, and size of cracks [68].

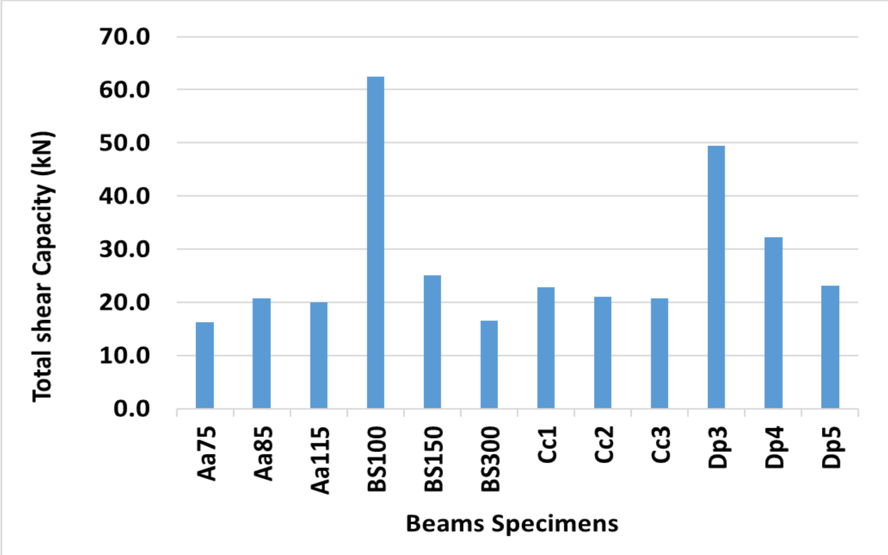

Fig. 18 Shear Capacity Values (V_{tr}) of all Specimen Beams.

3.6.Shear Capacity-Curvature Ductility Relationship

Curvature ductility is essential in structural engineering for RC beams, showing their ability to endure deformations without failing, crucial for seismic events and heavy loads. Ductility in curvature indicates the beam's energy absorption and release through plastic deformations, often assessed by comparing maximum curvature to yield curvature [69, 70]. The process of defining the ductility of curvature involves determining the relationship between the bending moment and the curvature of the beam. This relationship is determined by examining the cross-section of the beam, considering the nonlinearity of the material and strain compatibility. The curvature ductility factor (μϕ) can be calculated using the following equation [71, 72]:

$$\mu_\phi = \phi_u / \phi_y \quad (14)$$

Figure 19 illustrates how to determine the curvature ductility factor from the moment-curvature relationship.

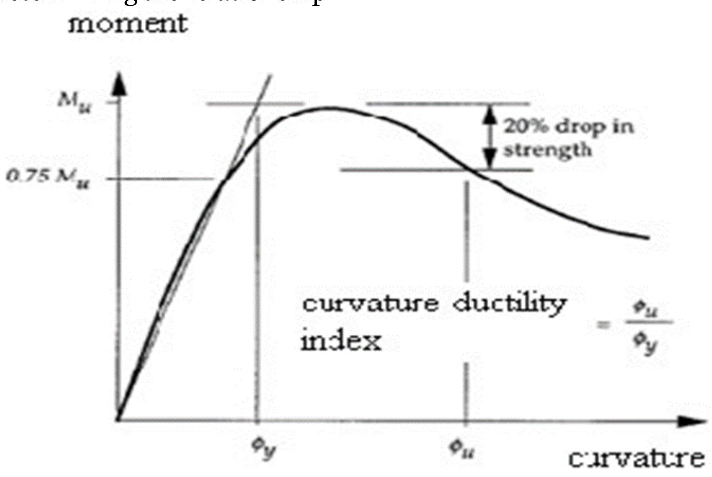

Fig. 19 Definition of Curvature Ductility Index (Desai et al., 2013).

The Moment-Curvature Curve Method illustrates the correlation between moment and curvature in a structural element, with the yield point marking the shift from elastic to plastic behavior, signifying the onset of plastic deformation [74]. The practical way to find the yield curvature is usually defined as 0.75 times the ultimate moment (Mu) following failure when the curve decreases. This method is widely acknowledged by various researchers ([73, 75]). The curvature ductility index values for all beams examined are tabulated in Table 8, which are derived from Fig. 17. Figure 20 shows the relationship between shear capacity and curvature ductility index for beam specimens in each group. This analysis concentrates on the primary aim of the thesis, which is to investigate the characteristics, extent, and consequences of these relationships.

Table 9 Curvature Ductility Index of All Beams Tested.

Speci.	ϕ_y (rad)	ϕ_u (rad)	μ_ϕ
Aa75*	1.6041E-05	4.9602E-05	3.092
Aa85	1.5197E-05	8.8229E-05	5.806
Aa115	1.3499E-05	8.8731E-05	6.573
BS100*	1.5189E-05	8.8207E-05	8.807
BS150	0.00001308	9.7619E-05	7.463
BS300	1.6008E-05	5.2805E-05	3.299
Cc1*	1.4108E-05	3.1459E-05	2.230
Cc2	1.2831E-05	3.4334E-05	2.676
Cc3	1.5611E-05	8.8229E-05	5.652
Dp3*	1.272E-05	0.00012881	10.127
Dp4	1.6217E-05	7.3169E-05	4.512
Dp5	1.9381E-05	3.5048E-05	1.808

* These are the control samples for each group.

Reviewing the figure for Group A, the ratio of shear span to effective depth (a/d) influences shear capacity and curvature ductility. A higher curvature ductility leads to increased shear capacity because of the higher a/d ratio. This shift from sudden to warning failure modes aligns with structural engineering goals. The study found a direct, nonlinear relationship between the curvature ductility and shear capacity of the beams in group B, which were equipped with three shear reinforcement values. This relationship indicates that an increase in curvature ductility results in an increase in shear capacity. It is beneficial as it promotes a non-sudden failure mode, which is desirable for the structural behavior of members. The relationship between group C beam samples and the impact on concrete strength was unclear. Two reasons: close strength values (50.3, 55, 65 MPa) with no significant difference, and complex concrete compositions hindering behavior assessment [76]. The results are not distinctive and can be vaguely described as inversely linear. In conclusion, group D in this study examined variation in longitudinal reinforcement amount as a variable. It showed the same three values as other groups, with a linear and positive relationship due to steel's consistent nature influencing structural behavior [77-80].

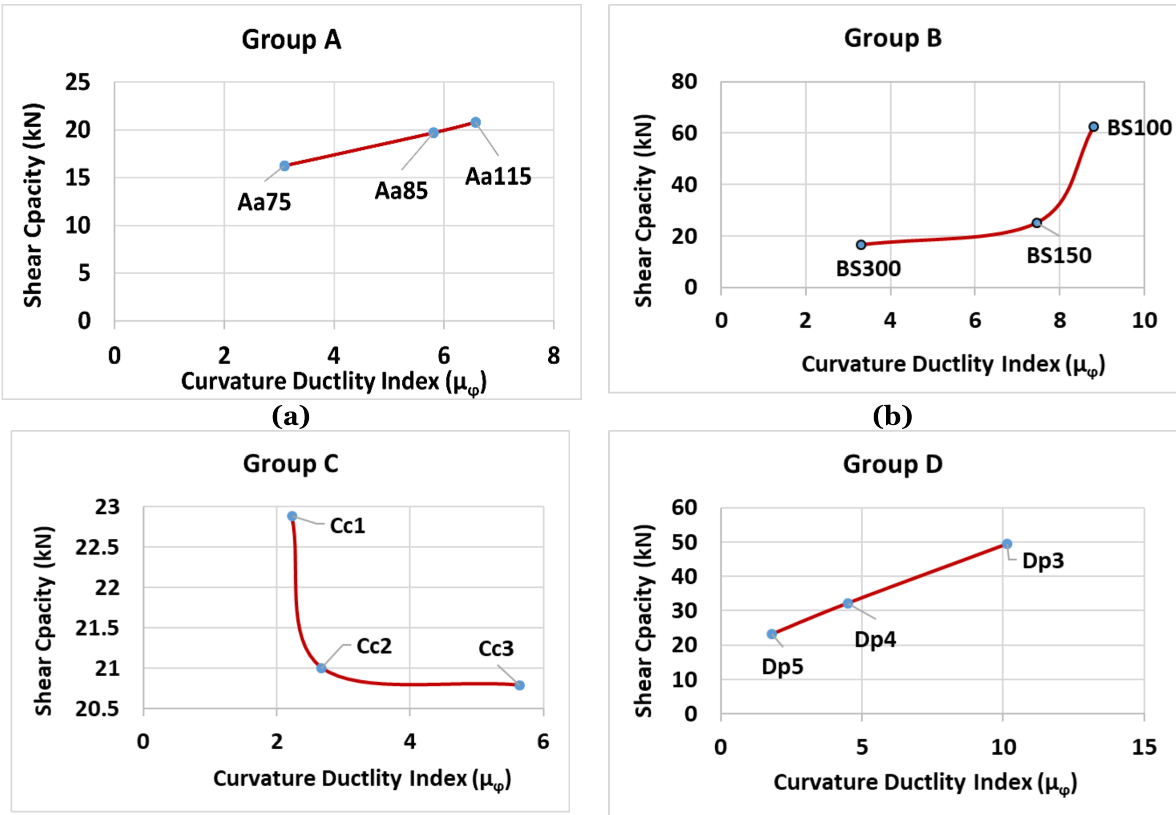

(c) (d)

Fig. 20 Shear Capacity-Curvature Ductility Relationships of All Specimen Beams.

4.CONCLUSIONS

The main conclusions of the present study could be summarized as follows:

- A higher shear span to effective depth ratio (a/d) in a concrete beam increased its ductility and flexural deformability by enhancing deformability and promoting widespread cracking.
- Increasing the shear span to effective depth ratio (a/d) resulted in higher energy absorption and larger deformations during loading.
- Higher shear span-depth ratios (a/d) improved beam moment and deformability pre-failure by enhancing flexural deformability, allowing for better stress redistribution and increased curvature capacity.
- Increasing the space between stirrups potentially reduces the ultimate curvature value, shear capacity, and curvature ductility of the beams, which could increase their susceptibility to abrupt failure.
- Increasing the spaces between stirrups can limit the appearance of flexural cracks to some extent by reducing the confinement on the concrete, allowing it to experience a more uniform stress distribution, which can lower stress concentrations and reduce crack initiation or severity.
- Enhancing the compressive strength of the concrete mix increases curvature ductility by promoting deformability and distributed cracking. This improvement boosted the beam's flexural deformability without significantly affecting its shear capacity.
- Increasing concrete's compressive strength reduced flexural crack widths and delayed shear cracks in reinforced beams, as it boosted stiffness and load capacity, enhancing crack resistance.
- Increasing flexural reinforcement at the top (tension zone) decreases the curvature ductility of the beams, making them more prone to sudden failure due to their reduced ability to bend and redistribute load as stress increases, and it also reduces their shear capacity.
- Increasing flexural reinforcement in concrete beams narrowed flexural cracks and made them more closely spaced.
- Diagonal shear cracks commonly appeared in the samples, indicating a potential failure of the concrete to resist shear. This behavior is mainly due to their alignment with flexural cracks, which has sped up their formation.

ACKNOWLEDGEMENTS

The authors appreciate the support provided for this research by the Civil Engineering Department at the College of Engineering, Tikrit University.

NOMENCLATURE

a	Shear span, mm
A_{sw}	Area of one stirrup, mm²
Av	Area of shear steel, mm²
b	Width of section beam, mm
c_o	Coefficient related to steel type, axial loading, and concrete strength
d	Effective depth, mm
d'	Spacing between LVDTs, mm
d_b	Diameter of longitudinal reinforcement, mm
d_g	Max aggregate size, mm
D_{fl}	Distance of First flexural crack from the joint, mm
D_{sh}	Distance of First shear crack from the joint, mm
E_s	Modulus of elasticity of steel, MPa
f'_c	Compressive strength of concrete, MPa
f_y	Yield strength of longitudinal reinforcement, MPa
f_{vy}	Yield strength of shear reinforcement, MPa
h	Height of section beam, mm
L_p	Plastic Hinge Length, mm
P_f	Load at first flexural crack, kN
P_{sh}	Load at First shear crack, kN
P_u	Ultimate Load, kN
s	Spacing between stirrups, mm
SG	Strain gauge
V_{cr}	Residual shear capacity of concrete, kN
V_{sn}	Nominal shear strength, kN
V_{sr}	Residual capacity of shear steel, kN
V_{sw}	Shear strength provided by shear reinforcement (Stirrups contribution), kN
V_{tr}	Total residual shear capacity of specimens, kN
z	Distance from the critical section to the point of contra flexure, mm
δ_{bott}	Horizontal displacement of the LVDT at the bottom, mm
δ_{fl}	Deflection at first flexural Crack, mm
δ_{sh}	Deflection at First shear crack, mm
δ_{top}	Horizontal displacement of the LVDT at the top, mm
δ_u	Deflection at the ultimate load, mm
ϕ_{fl}	Curvature value at the first flexural crack load, rad/mm
Greek symbols	
ϕ_{sh}	Curvature value at the first diagonal shear crack load, rad/mm
ϕ_u	Curvature value at the ultimate load, rad/mm
ϕ_y	Curvature at yielding, rad/mm
μ_ϕ	Curvature ductility index
θ_t	Total rotation of slab strip (beam), rad
$\theta_{elastic}$	Rotation at elastic deformation, rad
$\theta_{inelastic}$	Rotation at plastic deformation, rad
ϵ_s	Steel strain
σ_s	Steel stress, MPa
σ_{sw}	Stress for a single stirrup, MPa

REFERENCES

[1] Gjørv OE. **High-Strength Concrete**. *Developments in the formulation and reinforcement of concrete* 2008; 79–97.

[2] Natt L. **Chapter 6 High Strength Concrete**. 2018. Available from: https://www.researchgate.net/publication/326689280_Chapter_6_High_strength_concrete.

[3] Resende HF, Arroyo FN, Reis ED, Chahud E, Santos HF, Linhares JAT, Azevedo ARG, Christoforo AL, Branco LAMN. **Estimation of Physical and Mechanical Properties of High-Strength Concrete with Polypropylene Fibers in High-Temperature Condition**. *Journal of Materials Research and Technology* 2023; **24**: 8184–8197.

[4] Mendis P. **Design of High-Strength Concrete Members: State-of-The-Art**. *Progress in Structural Engineering and Materials* 2003; **5**(1): 1–15.

[5] Cavagnis F, Ruiz MF, Muttoni A. **Shear Failures in Reinforced Concrete Members Without Transverse Reinforcement: An Analysis of The Critical Shear Crack Development on The Basis of Test Results**. *Engineering Structures* 2015; **103**: 157–173.

[6] Ibraheem M, Rasheed M. **Shear Capacity of Reinforced Concrete Beams Without Shear Reinforcement: Review**. *Journal of Engineering and Sustainable Development* 2023; **27**(5): 580–595.

[7] Ullah N, Usman M, Farooq SH, Ashraf W, Hanif A. **Effect of Steel and Concrete Thickness on Shear Strength of Square Concrete Filled Double Skin Tubular Beams**. *Case Studies in Construction Materials* 2021; **14**: e00478.

[8] Shi X, Zhang Z, Li Z, Lou X. **Influencing Factors of Shear Capacity of Concrete Beam Reinforced With GFRP**. *Journal of Southwest Jiaotong University* 2010; **23**(6): 898-904.

[9] Bayrak O, Sheikh SA. **Plastic Hinge Analysis**. *Journal of Structural Engineering* 2001; **127**(9): 1092–1100.

[10] Zhao XM, Wu YF, Leung AYT. **Analyses of Plastic Hinge Regions in Reinforced Concrete Beams Under Monotonic Loading**. *Engineering Structures* 2012; **34**: 466–482.

[11] Zhao X-M, Wu Y, Leung AYT. **Analyses of Plastic Hinge Regions in Reinforced Concrete Beams Under Monotonic Loading**. *Engineering Structures* 2012; **34**: 466–482.

[12] Baker ALL. **The Ultimate-Load Theory Applied to the Design of Reinforced and Prestressed Concrete Frames**. 1st Edition, London: Concrete Publications; 1956.

[13] Sawyer HA. **Design of Concrete Frames for Two Failure Stages**. *Special Publication* 1965; **12**: 405-437.

[14] Corley W. **Rotational Capacity of Reinforced Concrete Beams**. *Journal of the Structural Division* 1966; **92**(5): 121–146.

[15] Mattock Alan. **Discussion of Rotational Capacity of Reinforced Concrete Beams**. *Journal of the Structural Division* 1967; **93**(2): 519–522.

[16] Paulay T, Priestley MJN. **Seismic Design of Reinforced Concrete and Masonry Buildings**. 1st Edition, New York: John Wiley and Sons, Inc.; 1992.

[17] Panagiotakos T, Fardis M. **Deformation of Reinforced Concrete Members at Yielding and Ultimate**. *Structural Journal* 2001; **98**(2): 135-148.

[18] Stringer DC. **The Elastic-Plastic Behaviour of Restrained Columns**. Ph.D. Thesis. University of Manchester; Manchester, United Kingdom; 1972.

[19] Iwankiw NR. **Ultimate Strength Considerations for Seismic Design of The Reduced Beam Section (Internal Plastic Hinge)**. *Engineering Journal* 1997; **34**(1): 3–16.

[20] Rao TM, Srikar N, Reddy GS, Praveen B. **Ductility of Reinforced Concrete Beams**. *CVR Journal of Science and Technology* 2015; **9**: 7–12.

[21] Priestley MJN. **Displacement-Based Seismic Assessment of Reinforced Concrete Buildings**. *Journal of Earthquake Engineering* 1997; **1**(1): 157–192.

[22] Tomlinson D, Fam A. **Performance of Concrete Beams Reinforced with Basalt FRP For Flexure and Shear**. *Journal of Composites for Construction* 2015; **19**(2): 04014036.

[23] Yuan F, Pan J, Leung C. **Flexural Behaviors of ECC and Concrete/ECC Composite Beams Reinforced with Basalt Fiber-Reinforced Polymer**. *Journal of Composites for Construction* 2013; **17**: 591–602.

[24] Arowojolu O, Ibrahim A, Almakrab A, Saras N, Nielsen R. **Influence of Shear Span-To-Effective Depth Ratio on Behavior of High-Strength Reinforced Concrete Beams**. *International Journal of Concrete Structures and Materials* 2021; **15**(1): 1–12.

[25] Yazdanbakhsh A, Tian Y. **Shear Performance of Reinforced Concrete Beams Incorporating Stiff Slender Elements**. *Construction and Building Materials* 2019; **222**: 263–277.

[26] Słowik M. **The Analysis of Failure in Concrete and Reinforced Concrete Beams with Different Reinforcement Ratio**. *Archive of Applied Mechanics* 2019; **89**: 885–895.

[27] Caglar N, Demir A, Ozturk H, Akkaya A. **A New Approach to Determine the Moment-Curvature Relationship of Circular Reinforced Concrete Columns**. *Computers and Concrete, An International Journal* 2015; **15**(3): 321–335.

[28] Cladera A, Marí AR. **Experimental Study on High-Strength Concrete Beams Failing in Shear**. *Engineering Structures* 2005; **27**(10): 1519–1527.

[29] Mardookhpour A. **Evaluation of Codes and Equation for Prediction Shear Capacity in HSC Beams Without Shear Reinforcements**. *World Journal of Engineering* 2012; **9**(1): 57–62.

[30] Nogueira CG, Rodrigues ID. **Ductility Analysis of RC Beams Considering the Concrete Confinement Effect Produced by The Shear Reinforcement: A Numerical Approach**. *Latin American Journal of Solids and Structures* 2017; **14**(13): 2342–2372.

[31] Hamid NAA, Ibrahim A, Thamrin R, Hamid HA. **Effect of Longitudinal Reinforcement Ratio on Shear Capacity of Concrete Beams with GFRP Bars**. *InCIEC 2015: Proceedings of the International Civil and Infrastructure Engineering Conference* 2016; 587–599.

[32] Sayhood EK, Mohammed NS, Hilo SJ, Salih SS. **Comprehensive Empirical Modeling of Shear Strength Prediction in Reinforced Concrete Deep Beams**. *Infrastructures* 2024; **9**(4): 67.

[33] Nguyen NT, Nguyen TK, Du DH, Nguyen DN. **Finite-Element Analysis of RC Beams Strengthened with CFRP U-Wraps**. *Mechanics of Composite Materials* 2022; **58**(4): 567–584.

[34] Tamayo JLP, Garcia GO. **Reassessment of the Flexural Behavior of High-Strength Reinforced Concrete Beams Under Short-Term Loads**. *SN Applied Sciences* 2021; **3**(2): 204.

[35] ASTM C. **C150/CC150M-19A Standard Specification for Portland Cement**. ASTM International, West Conshohocken, PA; 2019.

[36] ASTM C. **C778-17 Standard Specification for Standard Sand**. ASTM International, West Conshohocken, PA; 2017.

[37] ASTM C. **C33/CC33M-18 Standard Specification for Concrete Aggregates**. ASTM International, West Conshohocken, PA; 2018.

[38] ASTM C. **C-494/C-494M Standard Specification for Chemical Admixtures for Concrete, Type F**. ASTM International, West Conshohocken, PA; 2019.

[39] Mazloom M, Ramezanianpour AA, Brooks JJ. **Effect of Silica Fume on Mechanical Properties of High-Strength Concrete**. *Cement and Concrete Composites* 2004; **26**(4): 347–357.

[40] ASTM C. **ASTM C 1240–05: Standard Specification for Silica Fume Used in Cementitious Mixtures**. ASTM International, West Conshohocken, PA; 2005.

[41] Iraqi Standard Specification No.1703 for Portland Cement. Central Organization for Standardization and Quality Control, Baghdad, Iraq; 1992.

[42] ASTM A. **A615 Standard Specification for Deformed and Plain Carbon-Steel Bars for Concrete Reinforcement**. ASTM International, West Conshohocken, PA; 2018.

[43] EN BS. **8500-1. Concrete Complementary British Standard to BS EN 206-1-Part 1: Method of Specifying and Guidance for The Specifier**. British Standards Institution, London; 2006.

[44] Hossein SM, Shariatmadar H. **Enhancement of Seismic Performance of Beam-Column Joint Connections Using High Performance Fiber Reinforced Cementitious Composites**. *Construction and Building Materials* 2018; **180**: 665–680.

[45] Hu B, Kundu T. **Seismic Performance of Interior and Exterior Beam–Column Joints in Recycled Aggregate Concrete Frames**. *Journal of Structural Engineering* 2019; **145**(3): 04018262.

[46] Hu B, Wu YF. **Effect of Shear Span-to-Depth Ratio on Shear Strength Components of RC Beams**. *Engineering Structures* 2018; **168**: 770–783.

[47] Najafgholipour MA, Dehghan SM, Dooshabi A, Niroomandi A. **Finite Element Analysis of Reinforced Concrete Beam-Column Connections with Governing Joint Shear Failure Mode**. *Latin American Journal of Solids and Structures* 2017; **14**: 1200–1225.

[48] Said SH, Razak HA. **Structural Behavior of RC Engineered Cementitious Composite (ECC) Exterior Beam–Column Joints Under Reversed Cyclic Loading**. *Construction and Building Materials* 2016; **107**: 226–234.

[49] Shafaei J, Hosseini A, Marefat MS, Ingham JM. **Rehabilitation of Earthquake Damaged External RC Beam-Column Joints by Joint Enlargement Using Prestressed Steel Angles**. *Earthquake Engineering and Structural Dynamics* 2017; **46**(2): 291–316.

[50] Committee A. **ACI 318-19: Building Code Requirements for Structural Concrete and Commentary**. American

Concrete Institute: Farmington Hills, MI, USA; 2019.

[51] ASTM C. **C 39M-03 Standard Test Method for Compressive Strength of Cylindrical Concrete Specimens**. ASTM International, West Conshohocken, PA; 2003.

[52] ASTM C. **C 78-04 Standard Test Method for Flexural Strength of Concrete (Using Simple Beam with Four-Point Loading)**. ASTM International, West Conshohocken, PA; 2004.

[53] BS 1881: Part 116. **Method for Determination of Compressive Strength of Concrete Cubes**. British Standards Institution, London; 1983.

[54] Corrado M, Ventura G, Carpinteri A. **Experimental Evidences of Flexural to Shear to Crushing Failure Mode Transition in Reinforced Concrete Beams Without Stirrups**. *Engineering Structures* 2022; **271**: 114896.

[55] Kim SW, Han DS, Kim KH. **Evaluation of Shear Effect on Deflection of RC Beams**. *Applied Sciences* 2021; **11**(16): 7690.

[56] Li W, Huang X, Liu X, Wen T, Jing C, Li L. **Flexural Performance of Reinforced Concrete Beams Strengthened with a Novel High-Strength and High-Toughness Epoxy Mortar Thin Layer**. *Applied Sciences* 2024; **14**(10): 3999.

[57] Zhang JP. **Diagonal Cracking and Shear Strength of Reinforced Concrete Beams**. *Magazine of Concrete Research* 1997; **49**(178): 55–65.

[58] Kim W, White RN. **Hypothesis for Localized Horizontal Shearing Failure Mechanism of Slender RC Beams**. *Journal of Structural Engineering* 1999; **125**(10): 1126–1135.

[59] Dok G, Ozturk H, Demir A. **Determining Moment-Curvature Relationship of Reinforced Concrete Columns**. *The Eurasia Proceedings of Science Technology Engineering and Mathematics* 2017; **9**(1): 52-58.

[60] Aules WA, Rad F, Dusicka P, Schumacher T, Zareh H. **Behavior of Non-Ductile Slender Reinforced Concrete Columns Retrofit by CFRP under Cyclic Loading**. Ph.D. Thesis. Portland State University; Portland, United States; 2019.

[61] Kwak HG, Kim SP. **Nonlinear Analysis of RC Beams Based on Moment–Curvature Relation**. *Computers and Structures* 2002; **80**(7–8): 615–628.

[62] Wight JK, MacGregor JG. **Reinforced Concrete**. 6th Edition, UK: Pearson Education; 2016.

[63] Hakim J, Mhaya A, Ibrahim M, Mohammadhasani M, Mokhatar S, Paknahad M, Kamarudin A, Taylor G. **A Pioneering Approach to Predicting the Shear Strength of RC Beams by Employing Artificial Intelligence Techniques**. *Civil Engineering and Architecture* 2023; **12**: 218–230.

[64] Rodrigues RV, Muttoni A, Ruiz MF. **Influence of Shear on Rotation Capacity of Reinforced Concrete Members Without Shear Reinforcement.** *ACI Structural Journal* 2010; **107**(5): 516-525.

[65] Kheyroddin A, Naderpour H. **Plastic Hinge Rotation Capacity of Reinforced Concrete Beams**. *International Journal of Civil Engineering* 2007; **5**(1): 30-47.

[66] Hibbeler RC. **Mechanics of Materials**. 10th Edition, United States: Pearson; 2016.

[67] López AM, Sosa PFM, Senach JLB, Prada MÁF. **Influence of the Plastic Hinge Rotations on Shear Strength in Continuous Reinforced Concrete Beams with Shear Reinforcement**. *Engineering Structures* 2020; **207**: 110242.

[68] Yang Y, Yang H, Fan Z, Mu Z. **Crack Propagation Law of Reinforced Concrete Beams**. *Applied Sciences* 2024; **14**(1): 446.

[69] Arslan G, Cihanli E. **Curvature Ductility Prediction of Reinforced High-Strength Concrete Beam Sections**. *Journal of Civil Engineering and Management* 2010; **16**(4): 462–470.

[70] Olivia M, Mandal P. **Curvature Ductility of Reinforced Concrete Beam**. *Journal of Civil Engineering* 2005; **6**(1): 1–13.

[71] Bazan JL, Fernandez-Davila VI. **Evaluation of the Experimental Curvature Ductility of RC Beams Externally Strengthened with CFRP Bands.** *Structures* 2020; **26**: 1010–1020.

[72] Lee H-J. **Evaluation on Moment-Curvature Relations and Curvature Ductility Factor of Reinforced Concrete Beams with High Strength Materials**. *Journal of the Korea Concrete Institute* 2013; **25**(3): 283–294.

[73] Desai Pallavi MT, Rajan Professor A. **Seismic Performance of Soft Storey Composite Column**. *International Journal of Scientific and Engineering Research* 2013; **4**(1): 1-5.

[74] Haytham B, Amar K. **Curvature Ductility of High Strength Concrete Beams**. *Journal of Materials and Engineering Structures* 2017; **4**(3): 155-167.

[75] Park R. **Ductility Evaluation from Laboratory and Analytical Testing**. *Proceedings of the 9th World Conference on Earthquake Engineering* 1988; **8**: 605–616.

[76] Mehta PK, Monteiro PJM. **Concrete: Microstructure, Properties, and Materials**. 4th Edition, New York: McGraw-Hill Education; 2014.

[77] Zerfu K, Ekaputri JJ. **The Effect of Reinforcement Ratio on The Flexural Performance of Alkali-Activated Fly Ash-Based Geopolymer Concrete Beam**. *Heliyon* 2022; **8**(12): e12015.

[78] Ibraheem OF, Abdullah HA. **Behavior of Steel Beams Subjected to Bending and Shear Loading Under Localized Fire Conditions**. *Tikrit Journal of Engineering Sciences* 2022; **29**(3): 82–90.

[79] Alobaidy QNA, Abdulla AI, Al-Mashaykhi M. **Shear Behavior of Hollow Ferrocement Beam Reinforced by Steel and Fiberglass Meshes**. *Tikrit Journal of Engineering Sciences* 2022; **29**(4): 27–39.

[80] Abdullah AI, Lateef AM. **Novel Torsional Reinforcement of Concrete Beams Utilizing Cross-Rod Steel Reinforcement**. *Tikrit Journal of Engineering Sciences* 2023; **30**(3): 49–58.